LBL-21508
Preprint c.2

Lawrence Berkeley Laboratory

UNIVERSITY OF CALIFORNIA

RECEIVED
LAWRENCE
BERKELEY LABORATORY

AUG 12 1986

LIBRARY AND
DOCUMENTS SECTION

Materials & Molecular Research Division

Submitted to Journal of the
American Ceramic Society

CREEP-SINTERING AND MICROSTRUCTURE DEVELOPMENT OF HETEROGENEOUS MgO COMPACTS

M. Lin, M.N. Rahaman, and L.C. De Jonghe

May 1986

TWO-WEEK LOAN COPY
This is a Library Circulating Copy
which may be borrowed for two weeks.

Prepared for the U.S. Department of Energy under Contract DE-AC03-76SF00098

LBL-21508 c.2

DISCLAIMER

This document was prepared as an account of work sponsored by the United States Government. While this document is believed to contain correct information, neither the United States Government nor any agency thereof, nor the Regents of the University of California, nor any of their employees, makes any warranty, express or implied, or assumes any legal responsibility for the accuracy, completeness, or usefulness of any information, apparatus, product, or process disclosed, or represents that its use would not infringe privately owned rights. Reference herein to any specific commercial product, process, or service by its trade name, trademark, manufacturer, or otherwise, does not necessarily constitute or imply its endorsement, recommendation, or favoring by the United States Government or any agency thereof, or the Regents of the University of California. The views and opinions of authors expressed herein do not necessarily state or reflect those of the United States Government or any agency thereof or the Regents of the University of California.

CREEP-SINTERING AND MICROSTRUCTURE DEVELOPMENT OF HETEROGENEOUS MgO COMPACTS

M. Lin, M. N. Rahaman* and L. C. De Jonghe*
Materials and Molecular Research Division
Lawrence Berkeley Laboratory
University of California
Berkeley, CA 94720

Abstract

Simultaneous creep and densification and the microsructure development of magnesium oxide powder compacts were studied at 1250°C and for applied stresses of up to 0.25 MPa. Die pressing the powder into compacts with a relative green density of $\sim$0.45 led to an approximately bimodal distribution of pores, with one fraction having sizes of the order of ten times the (initial) particle size and the other fraction having pore sizes of the order of the particle size. The presence of the large pores in turn gave rise to rather unusual sintering effects. After first decreasing with relative density, ρ, the densification rate, $d\rho/dt$, and the creep rate, $d\varepsilon/dt$, then increased dramatically for $0.6 < \rho > 0.75$. This range of ρ corresponded to the stage of microstructure development when grain growth and pore coalescence of the smaller pores have created a more uniform pore distribution. Above $\rho \sim 0.75$, both $d\rho/dt$ and $d\varepsilon/dt$ again decreased with ρ. These trends in the densification behaviour are discussed in terms of material parameters such as the equilibrium dihedral angle and the pore coordination number.

Presented in part at the Pacific Coast Regional Meeting, the American Ceramic Society, October 1985 (Paper 14-B-85P). Supported by the Division of Materials Science, Office of Basic Energy Sciences, U. S. Department of Energy, under Contract No. DE-AC03-76SF00098.

*Member, The American Ceramic Society.

I. INTRODUCTION

Magnesium oxide has been the subject of numerous studies on densification behaviour, creep, and grain growth. Accordingly, it was considered a good model material for use in experiments involving the loading dilatometer technique.[1-4] In this technique, the application of a small, controlled, uniaxial stress to a sintering compact allows the simultaneous creep and densification to be investigated. A key benefit is that the creep kinetics, can be separated from the volumetric densification kinetics.

A brief summary of past work on the hot-pressing, creep, and conventional sintering (i.e. without external, applied pressure) of MgO has been provided by Vieira and Brook.[5] Basically, the kinetics of these processes are dependent on a number of factors that include temperature, applied stress, grain size, and purity. For powder having a purity of 99.8 - 99.9% MgO, and a grain size less than 1μm, the kinetics of conventional sintering between ∿1250 and 1650°C are believed to be controlled by lattice diffusion of the magnesium ion.[6-8] The isothermal grain growth during conventional sintering between 1450 and 1650°C has been found to obey a quadratic growth law, in which the square of the grain size is proportional to time.[7]

The effects of grain growth on sintering and creep kinetics have been considered in a number of models. The treatments predict that the densification rate, $d\rho/dt$, and the creep rate, $d\varepsilon/dt$, have a functional dependence on grain size, G, of the form G^{-m}, where m depends on the mechanism of mass transport. In the conventional sintering of oxide

ceramics, these mechanisms are usually diffusional processes. The exponent m equals 3 for grain boundary diffusion (Coble Creep[9]) and m equals 2 for lattice diffusion (Nabarro-Herring Creep[10, 11]). Since grain growth causes an increase in the diffusion paths, according to these kinetic models the densification rate should decrease monotonically with time or density. This type of behavior has generally been observed in numerous studies.

Lange[12] has considered certain aspects of the interaction between grain growth and densification from a predominantly thermodynamic-geometric viewpoint, building on concepts first put forward by Kingery and Francois.[13] According to Kingery and Francois, only those pores with a coordination number, N, less than a critical value, N_c, are able to disappear during sintering. The value of N_c depends on the equilibrium dihedral angle, θ, and increases with θ. Lange, argued that normal grain growth can in certain respects be beneficial for sintering since it can lead to a reduction in the pore coordination number. That is, if the rate of grain growth exceeds that of pore growth, a time (or temperature) can be found that would reduce the coordination number of pores with $N > N_c$ to a value less than N_c.

Recently, De Jonghe et al[14] have considered the densification behaviour of a system consisting of large pores in a fine-grained, homogeneous matrix. They found that homogenization of the overall pore microstructure was possible due to grain growth driven pore coalescence of the finer pores, while the large pores grow less, thus leading to a more homogeneous microstructure. Conditions on parameters such as the initial grain size, the grain growth rate and the densification rate, were

identified for which micostructural homogeneity can be achieved before the end of the intermediate stage of sintering.

Hsueh and Evans[15] have developed a viscoelastic model to descibe the shrinkage rate of large pores in a fine-grained matrix, and have used it to predict trends in the densification rates and the pore shrinkage rates. A rapid rise in the densification rate is expected to occur when the pore size (of the large pores) has shrunk to a size that is of the order of the grain size, because of a substantial increase in the chemical potential gradient.

In this study, the simultaneous creep and densificaton behaviour of MgO powder compacts was studied using a loading dilatometer at 1250°C under applied stresses of up to 0.25 MPa. Initial experiments had shown that die-pressing of the powder 'as received' from the manufacturer resulted in a green compact containing an appreciable fracton of large pores in a fine-grained matrix. The effect of this green microstructure on the creep and densification behaviour was investigated by correlating the microstructure development with the creep and densification kinetics.

II. EXPERIMENTAL PROCEDURE

Magnesium oxide powder* was uniaxially pressed at ∿20 MPa into cylindrical compacts (6 mm diameter by 5mm) with a green relative density

*Reagent Grade, J. T. Baker Chemical Co., Phillipsburg, N. J.

of 0.45±0.01. These compacts were sintered in air, in a loading dilatometer[1] capable of operating at temperatures up to 1400°C with applied stresses of up to 0.25 MPa. After preliminary experiments, an isothermal sintering temperature of 1250°C was chosen since, at this temperature, an appreciable change in density could be obtained within a convenient time of ∿4 hours. Although the duration of most creep/sintering runs was ∿4 hours, a number of experiments were also conducted for times of up to 4 days.

In a typical experiment, the MgO compact was first placed in position in the loading dilatometer, and after the furnace had reached the working temperature, the sample was quickly introduced into the hot zone. When the sample had reached the sintering temperature, the load was applied rapidly (<5 sec.), and the axial shrinkage and temperature were recorded. The mass and dimensions of the compacts were measured before and after they were sintered, and the final density was measured using Archimedes' principle. In a separate set of experiments, sintering was terminated after times between 0 and 96 hours, and the dimensions of these compacts were measured using a micrometer.

The fracture surfaces, and polished and etched surfaces of samples sintered between 0 and 96 hr were examined using scanning electron microscopy. The preparation of polished surfaces involved vacuum impregnation with an epoxy resin, followed by polishing using diamond paste and non-aqueous lubricants. After burning off the resin at ∿350°C, the samples were thermally etched at 1200°C for 30 minutes. Average grain

sizes were measured by counting the number of grains traversed by straight lines of known length. The average grain size was taken as 1.5 times the average intercept length. The maximum estimated error in the average grain size measurements is ±15%. Equilibrium dihedral angles were obtained from a polished surface of a specimen sintered to a relative density of ∿0.85. About 100 measurements were made.

III. RESULTS

Figure 1 shows the smoothed average curves for the axial shrinkage, $\Delta L/L_0$, versus the logarithm of time, log t, for applied loads between 0 and 6N at 1250°C (L_0 = initial sample length, $\Delta L = L - L_0$, where L = instantaneous sample length). A load of 1N represents a stress of 35 kPa on the green compact and t = 0 represents the time at which the sample was inserted into the furnace. The sintering temperature was reached after t = 10 min. and the applied loads could be maintained to within ±1%. Each curve is the average of two runs under the same conditions and is reproducible to within ±2%. Weight losses after sintering for 4 hours was ∿3%. It is seen that at any time, $\Delta L/L_0$ increases with increasing load.

In these loading dilatometer experiments, the shrinkage of the compact is anisotropic. In order to evaluate the creep strain and the density, results for the radial shrinkage are also required. These results are shown in Fig. 2, where the axial shrinkage, $\Delta L/L_0$, is plotted vs the radial shrinkage, $\Delta D/D_0$ (D_0 = initial sample diameter and $\Delta D = D - D_0$, where D = instantaneous sample diameter). The $\Delta L/L_0$ values are approximately

proportional to $\Delta D/D_0$ and the slopes of the lines increase with increasing load.

A methodology described by Raj[16] and Figures 1 and 2 were used to separate the creep strain, ε, from the volumetric densification. Figure 3 shows the relative density, ρ, vs log t. Within the limits of experimental error, the values of ρ are almost independent of applied load. Figure 4 shows for ε vs log t, and it is seen that applied load has a systematic and pronounced effect on the creep behaviour. At any t, the values of ε increase with increasing load. The creep strains are relatively small (<5%) compared with those obtained in similar experiments on glass powder[17,18] for which creep strains of the order of 20% were observed.

Figure 5 shows the results for grain growth during sintering. The average grain size, G, normalized to the initial grain size, G_0, can be best fitted by a cubic growth law of the form

$$(G/G_0)^3 = 1 + kt \qquad (1)$$

where k is a constant equal to 2.7×10^{-2} min^{-1}. This is different from the quadratic growth law observed by Gupta[7] but is consistent with the grain growth dependence observed for a large number of oxides. The difference between these results and those of Gupta may be due to the much lower temperature used in this work. The mean value obtained for the equilibrium dihedral angle was 100° .

IV. DISCUSSION

As pointed out earlier in the analysis of the creep and densification results for CdO,[3] a more fundamental understanding of the creep and densification behaviour may be obtained by exploring the functional dependence of the creep rate, $\dot{\varepsilon}$, and the densification rate, $\dot{\rho}$, on relative density, ρ. Two complications are that first, the grain size increases with density due to grain growth, and second, the applied stress increases slightly with density due to the changing cross-sectional area during sintering. However, both effects can be easily compensated for. Considering first the densification results, in order to compensate for grain growth use may be made of an equation for the densification rate of the general form[3]

$$\dot{\rho} = \frac{BD\Omega}{k_B T} \frac{1}{GX_o^{m-1}} \Sigma \qquad (2)$$

where B is a geometrical constant, Σ is the driving force, or the sintering stress, D is the diffusivity, Ω is the molecular volume, k_B is the Boltzmann constant, T is the absolute temperature, and m is an exponent characteristic of the mechanism for densification. X_o is the neck radius, and provided all grain triple junctions are pores, is related to the grain size G by the equation[3]

$$X_o = G(A_e/A)^{1/2} = G/\phi^{1/2} \qquad (3)$$

where A is the total cross sectional area of the specimen and A_e is its actual, internal load-bearing area. The quantity ϕ is usually referred to as the stress intensification factor. For very inhomogeneous systems and

when all grain triple junctions do not contain pores, ϕ will contain additional microstructural information. Equation (2) may be simplified to give

$$\dot{\rho} = K_1 \Sigma \phi^{m-1}/G^m \qquad (4)$$

where K_1 is a constant at a fixed temperature. Compensation for grain growth can be made by use of a plot of log $(G^m\dot{\rho}/G_0^m)$ vs ρ, where the values for the grain size, G, at any time, t, corresponding to ρ (at time t) follows from Equation 1. For MgO the mass transort mechanism is expected to be lattice diffusion,[6-8] with the exponent m = 2. The correction for the change in applied stress due to the change in cross-sectional area is negligible for the densification results.

Figure 6 shows the results for the logarithm of the grainsize-compensated densification rate log $(G^2\dot{\rho}/G_0{}^2)$ vs ρ. A striking feature is that above $\rho \sim 0.6$, the grainsize-compensated densification rate <u>increases</u> with density. This feature is very unusual, and has not been reported before in the sintering of single-phase systems.

To compensate for grain growth in the analysis of the creep results, use may be made of an equation of the form[3]

$$\dot{\varepsilon} = K_2 \sigma_a^p \phi^{(m+1)/2}/G^m \qquad (5)$$

where K_2 is a constant, σ_a the applied stress and p is an exponent characteristic of the creep mechanism. For diffusional creep p = 1, and for these experiments where the applied stresses are small, the creep mechanism is likely to be the same as that for densification with m = 2.

Figure 7 shows the logarithm of the grain-size compensated creep rate log $(G^2\dot{\varepsilon}/G_0^2)$ vs ρ for the applied stresses shown. To compensate for the change in cross-sectional area of the specimen during sintering, each curve has been plotted at constant stress, using the results of Fig. 2 and the observed dependence of $\dot{\varepsilon}$ on stress. Similar to the observation for the densification results, above $\rho \sim 0.6$ the creep rates increase with density.

To investigate further the feature of the increase in the grain-size-compensated densification rate (and creep rate) with ρ above $\rho \sim 0.6$, experiments were performed for much longer times to cover a wider density range. Figure 8 shows the logarithm of the observed densification rate, log $\dot{\rho}$, and the logarithm of the grainsize-compensated densification rate, $\log(G^2\dot{\rho}/G_0^2)$ vs ρ for an applied stress of 0.2 MPa. It is seen that after first decreasing with ρ, log $(G^2\dot{\rho}/G_0^2)$ increases with ρ between $\rho \sim 0.6$ and 0.75. Above $\rho \sim 0.75$, log $(G^2\dot{\rho}/G_0^2)$ decreases with increasing ρ. The corresponding curves for the creep results, log $\dot{\varepsilon}$ and log $(G^2\dot{\varepsilon}/G_0^2)$ vs ρ are shown in Fig. 9. The behaviour of log $(G^2\dot{\varepsilon}/G_0^2)$ as a function of ρ is similar to that of log $(G^2\dot{\rho}/G_0^2)$.

Figure 10 shows the scanning electron micrographs of the polished and thermally etched surfaces of samples sintered for times of (a) 20 min, (b) 100 min, (c) 400 min and (d) 48 hours. A striking feature is the pronounced change in the homogeneity of the microstructures from Fig. 10(a) to Fig 10(d). The green compact contains an appreciable fraction of large pores, similiar to those shown in Fig. 10(a), embedded in a matrix of small grains. The diameters of these large pores are 10 - 20 times the particle size of the (unsintered) powder and are thought to arise primarily from the

agglomeration behaviour of the powder. During sintering, it appears that the large pores grow relatively slowly, while the small pores in the fine-grained matrix grow rapidly due to graingrowth-driven pore coalescence. This behaviour continues for at least 100 min, Fig. 10(b), where the pore diameters are 3-5 times the grain size of the matrix. After 400 min, Fig. 10(c), the grain and pore sizes of the matrix have increased to the stage where they are becoming comparable to the size of the 'large' pores initialy embedded in the matrix. Thus, in effect, the microstructure has evolved to a more homogeneous state.

As seen from Fig. 6, the increase in the grainsize-compensated densification rate with begins at $\rho \sim 0.6$, i.e. at $t \sim 200$ min. At this time, it is estimated that the average, cross-sectional coordination number N, of the large pores is ~ 6 to 8. It apears that normal grain growth has decreased the coordination number of the large pores such that at $t \sim 200$ min, N is less than the critical value, N_c, estimated at ~ 6 to 8 in 2-dimensional cross-section. Shrinkage of the large pores can now occur, and this leads to an increase in the densification rate (and the creep rate). The value of N_c of ~ 6 to 8 suggests an equilibrium dihedral angle of 90 to 110 degrees in good agreement with the value of 100 degrees obtained experimentally. These observations appear to support Lange[12], who argued that that normal grain growth might be beneficial for sintering since it leads to a reduction of the pore coordination number. It appears that these results cannot be explained by a change in the structure of the MgO grains, since between t = 100 and 400 min, Figs. 10(b) and 10(c), no change in the grain structure is observed.

When the large pores have shrunk to approximately the size of the matrix pores ($\rho \sim 0.75$, $t \sim 600$ min), the grainsize-compensated densification rate again starts to decrease with density. The compact microstructure has reached a much more homogeneous state and this persists even after long sintering times, Fig. 10(d).

It should be pointed out that for a green microstructure consisting of large pores in a fine-grained matrix, homogenization can only occur under specific conditions of temperature, graingrowth rate, and densification rate.[14]

V. FURTHER CONSIDERATIONS

The functional dependence of the stress intensification factor, ϕ, on the relative density, ρ, may be obtained from a plot of log $(G^2\dot{\varepsilon}/G_0^2)$ vs ρ (Fig. 8). It is seen that ϕ is a complicated function of ρ, due mainly to the drastic change in the microstructure for values of ρ between 0.6 and 0.75. Below $\rho \sim 0.6$, when the large pores do not take part in the densification process, and above $\rho \sim 0.75$ when the microstructure has reached a more uniform state, ϕ apears to be a simple exponential function of ρ. The nature of ϕ observed in these studies should be compared with the simple functional dependence observed for CdO[3]. For CdO over a wide density range between 0.5 and 0.9, ϕ is a simple exponential function of the form $\phi = \exp(aP)$, where a is a constant (=2.0) and P is the porosity. The difference in the nature of ϕ for MgO and CdO is a reflection of the striking difference in the uniformity of the microstructures of these two

materials. Fig. 11 shows SEM micrographs of the fracture surfaces of (a) a CdO compact sintered to $\rho \sim 0.65$ and (b) an MgO compact sintered to $\rho \sim 0.62$. The CdO microstructure is much more uniform and is free of very large pores.

Fig. 12 shows the average size of the large pores in the sample as a function of time. The sizes of the large pores were determined from scanning electron micrographs of polished surfaces. For the first part of the densification the average size of these large pores is nearly constant; they start to shrink at the onset of the densification and creep rate anomaly. Thus, the heterogeneous system studied here could, in its early stages, be considered to consist of inactive large pores, in a densifying fine pore matrix. If the inactive pore volume is P_i, then the overall stress intensification factor ϕ_a could be considered to consist of the matrix one, ϕ_m, corrected for the presence of the large pores. Thus, for the early part of densification, when the system is clearly bimodal

$$\phi_a = \frac{1}{(1-P_i)} \phi_m = \frac{1}{(1-P_i)} \exp\left(a_a (P-P_i)\right) \tag{6}$$

After homogenization has occured, in the later part of the densification, the stress intensification factor should again be:

$$\phi_b = \exp\left(a_b P\right) \tag{7}$$

Thus,

$$\phi_a/\phi_b = \frac{1}{(1-P_i)} \exp\left(-a_a P_i\right) \exp\left(P(a_a - a_b)\right) \tag{8}$$

An analysis of the evolution of ϕ for the heterogeneous compact should reflect this change.

ϕ derived from the data, assuming volume diffusion control, is shown in Fig. 13. Experimentally, the values for a_a and a_b are found to be: a_a = 17, a_b = 10. The value of P_i consistent with Eqn. (7) would be 0.25. It is clear from Fig. 13 that ϕ follows the expected trend. The ratio of ϕ_b/ϕ_a derived from the data, is also plotted in Fig. 13. This ratio should be consistent with the amount of inactive porosity, P_i. The volume fraction of the large pores, P_i, determined from sections of the sample in the early stage of densification is about 0.25. This agrees remarkably well with the value expected from the evolution of ϕ shown in Fig. 13. A further self-consistency in the relation of ϕ_a and ϕ_b should be observed when comparing the values of ϕ_a extrapolated to $P = P_i$ and of ϕ_b extrapolated to P = 0. The ratio $\phi_a (P = P_i)/\phi_b (P = 0)$ should be equal to $1/(1 - P_i)$, as follows from Eqns. 6 and 7. This indeed agrees well with the data shown in Fig. 13.

The analysis is thus consistent if the anomaly in the densification rates results from the switching of the microstructure from a bimodal pore distribution, with the large pores essentialy inactive, to a nearly homogeneous one.

The values of a_a and a_b are not equal, as is evident from Fig. 13. They are also larger than what would be expected on the basis of the Beere[19,20] and Viera and Brook[5] approximation for the dihedral angle of MgO. It is possible that the anisotropy of the particle shapes is the reason for these differences. Shape anisotropy and discrepancies between the pore distance and the grainsize should be expected to modify significantly the value of

α, since the pore shape does then no longer follow from the dihedral angle only and Eqn. 3 will need to be modified.

The sintering stress calculated from the ratio of the creep over the densification rate and from the values of shown in Fig. 13, has been shown in Fig. 14. Σ continuously decreases with porosity. This is indeed expected, since the densification is accompanied by significant pore growth. The results thus show clearly that the approximateley constant value for Σ found for the densification of CdO and ZnO should not be assumed to be constant in general.

VI. CONCLUSIONS

For heterogeneous MgO compacts containing an appreciable fraction of large pores in a fine-grained matrix, the densification rate, $d\rho/dt$, and the creep rate, $d\varepsilon/dt$, increase dramatically with relative density, ρ, between $\rho \sim 0.6$ and ~ 0.75. This increase in $d\rho/dt$ (and $d\varepsilon/dt$) may be attributed to the shrinkage of the large pores after some graingrowth has occured and homogenization of the microstructure has developed. Above $\rho \sim 0.6$, normal grain growth has decreased the pore coordination number, N, of the larger pores to a value below the critical value, N_c, so that these pores can shrink. The critical pore coordination number, N_c, is estimated to be ~ 6 to 8, suggesting an equilibrium dihedral angle of 90 to 110 degrees for the MgO powder used. This value of the dihedral angle is in good agreement with the experimentally measured value of 100 degrees.

The increase in $d\rho/dt$ and $d\varepsilon/dt$ at $\rho \sim 0.6$ is related to the disappearance of the microstructural heterogeniety, described by changes in the stress intensification factor, ϕ.

The stress intensification factor, ϕ, may also contain other microstructural information, in addition to the change in the load-bearing area.

Acknowledgment: M. Weiser is thanked for help with the computational analysis of the data.

REFERENCES

1. L. C. De Jonghe and M. N. Rahaman "A Loading Dilatometer", Rev. Sci. Instum., 55, [12] 2007-10 (1984).

2. M. N. Rahaman and L. C. De Jonghe, "Sintering of CdO Under Low Applied Stress", J. Am. Ceram. Soc., 67 [10] C-205-207 (1984).

3. M. N. Rahaman, L. C. De Jonghe, and R. J. Brook, "Effect of Shear Stress on Sintering", J. Am. Ceram. soc., 69 [1] 53-58 (1986).

4. M. N. Rahaman, L. C. De Jonghe and C. H. Hsueh, "Creep During Sintering of Porous Compacts", J. Am. Ceram. Soc., 69 [1] 58-60 (1986).

5. J. M. Vieira and R. J. Brook, "Hot-Pressing of High-Purity Magnesium Oxide", J. Am. Ceram. Soc. 67 [7] 450-54 (1984).

6. T. Vasilos and R. M. Spriggs, "Pressure Sintering Mechanisms and Microstructures for Alumina and Magnesia", J. Am. Ceram. Soc., 46 [10] 493-96 (1983).

7. T. K. Gupta, "Sintering of MgO: Densification and Grain Growth", J. Mater. Sci, 6, 25-32 (1971).

8. B. Wong and J. A. Pask, "Experimental Analysis of Sintering of MgO Powder Compacts", J. Am. Ceram. Soc., 62 [3-4] 141-46 (1979).

9. R. L. Coble, "Sintering Crystalline Solids: I", J. Appl. Phys. 32 [5] 787-92 (1961).

10. F. R. N. Nabarro, "Deformation of Crystals by Motion of Single Ions", pp. 75-90 in Report of a Conference on the Strength of Solids, University of Bristol, July 1947.

11. C. Herring, "Diffusional Viscosity of a Polycrystalline Solid", J. Apl. Phys., 21 [5] 437-45 (1950).

12. F. F. Lange, "Sinterability of Agglomerated Powders", J. Am. Ceram. Soc., 67 [2] 83-89 (1984).

13. W. D. Kingery and B. Francois, "Sintering of Crystalline Oxides, I. Interactions Between Grain Boundaries and Pores", pp. 471-98 in Sintering and Related Phenomena. Edited by G. C. Kuczynski, N. A. Hooton, and G. F. Gibbon. Gordon Breach, New York, 1967.

14. L. C. De Jonghe, M. N. Rahaman, and M. Lin, "The Role of Powder Packing in Sintering", unpublished work, LBL- 21620, May 1986.

15. C. H. Hsueh and A. G. Evans, "The Behaviour of Large Pores During Sintering and Hot-Pressing", submitted to J. Am. Ceram. Soc.

16. R. Raj, "Separation of Cavitation-Strain and Creep-Strain During Deformation", J. Am. Ceram. Soc., 65 [3] C-46 (1982).

17. M. N. Rahaman and L. C. De Jonghe, "Creep and Densification During Sintering of Glass Powder Compacts: I, Effect of Applied Stress and Temperature", submitted to J. Am. Ceram. Soc., LBL-20713, December 1985.

18. M. N. Rahaman, L. C. De Jonghe, and R. J. Brook, "Creep and Densification During Sintering of Glass Powder Compacts: II, Effect of Particle Size", submitted to J. Am. Ceram. Soc., LBL-20714, December 1985.

19. W. Beere "A Unifying Theory of the Stability of Penetrating Liquid Phases and Sintering Pores" Acta Metall., 23 [1] 131-38 (1975).

20. W. Beere "The Second Stage Sintering Kinetics of Powder Compacts" Acta Metall 23 [1] 139-45 (1975).

LIST OF FIGURES:

Figure 1: Smoothed average curves for the axial shrinkage vs time for loads shown (in newton) and at 1250°C.

Figure 2: The axial shrinkage as a function of the radial shrinkage for loads shown (in newton).

Figure 3: The relative density vs time for loads shown (in newton).

Figure 4: The creep strain vs time for loads shown (in newton).

Figure 5: The cube of the grain size normalized to the initial grain size, $(G/G_0)^3$, as a function of time.

Figure 6: The grainsize-compensated densification rate vs relative density.

Figure 7: The grainsize-compensated creep rate vs relative density.

Figure 8: The observed densification rate, $\dot{\rho}$, and the grainsize-compensated densification rate, $G^2\dot{\rho}/G_0^2$, vs relative density for an applied stress of 0.2 MPa.

Figure 9: The observed creep rate, $\dot{\varepsilon}$, and the grainsize-compensated creep rate, $G^2\dot{\varepsilon}/G_0^2$, versus relative density for an applied stress of 0.2 MPa.

Figure 10: Scanning electron micrographs of polished and thermally etched surfaces of samples sintered for times of (a) 20 min, (b) 100 min, (c) 400 min and (d) 48 hours.

Figure 11: Scanning electron micrographs of the fracture surfaces of (a) a CdO compact sintered to $\rho \sim 0.65$ and (b) an MgO compact sintered to $\rho \sim 0.62$.

Figure 12: The average size of the large pores in the sample vs time.

Figure 13: The stress intensification factor, ϕ, vs relative density.

Figure 14: The sintering stress vs relative density.

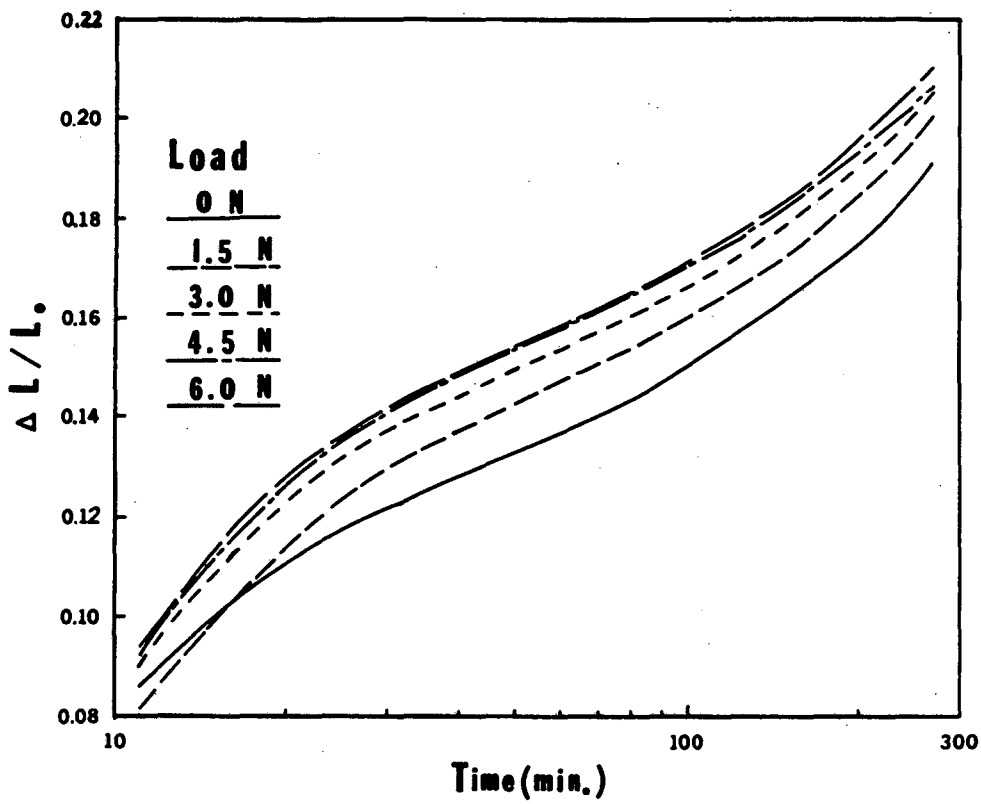

XBL 866-2189

Figure 1

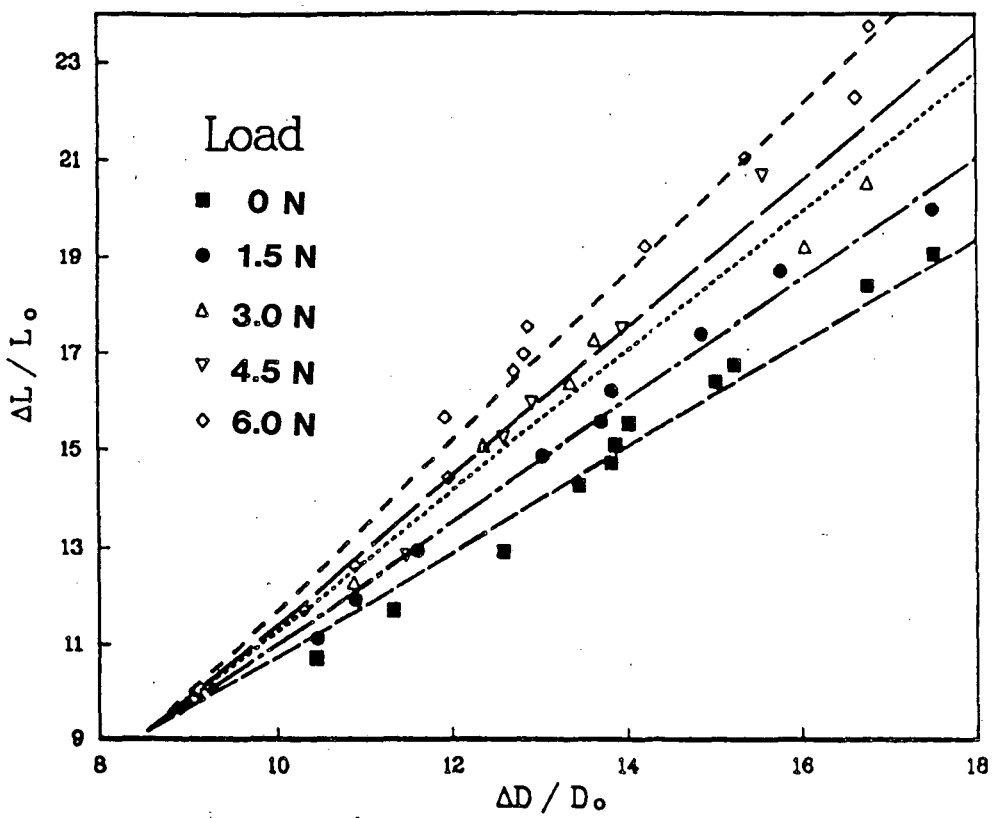

XBL 864-1656

Figure 2

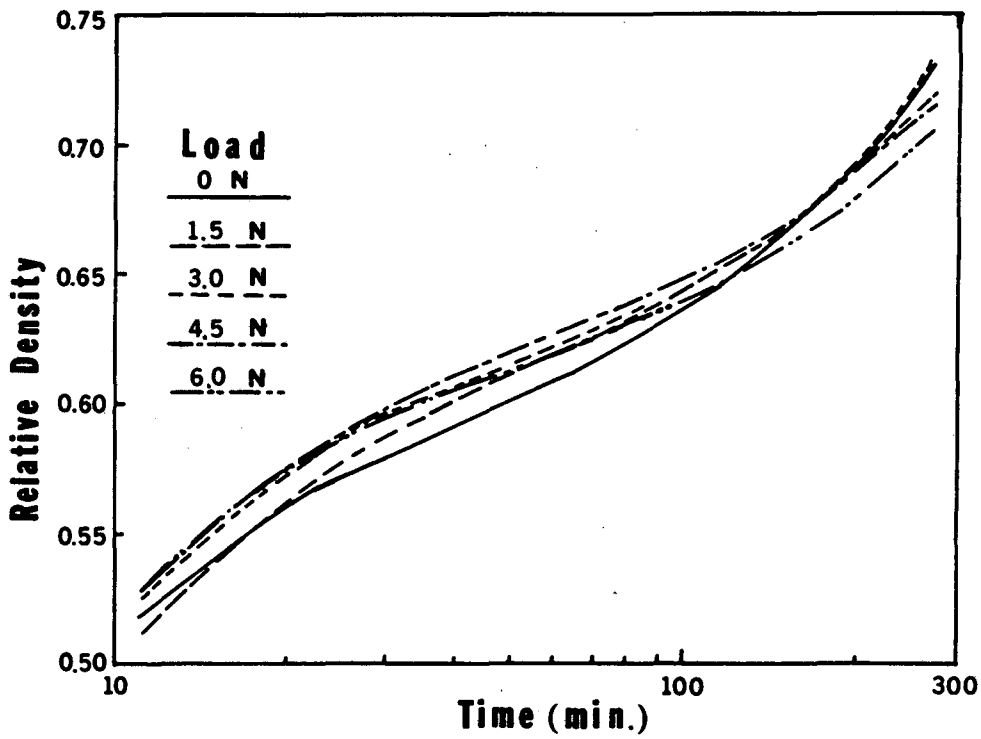

XBL 866-2190

Figure 3

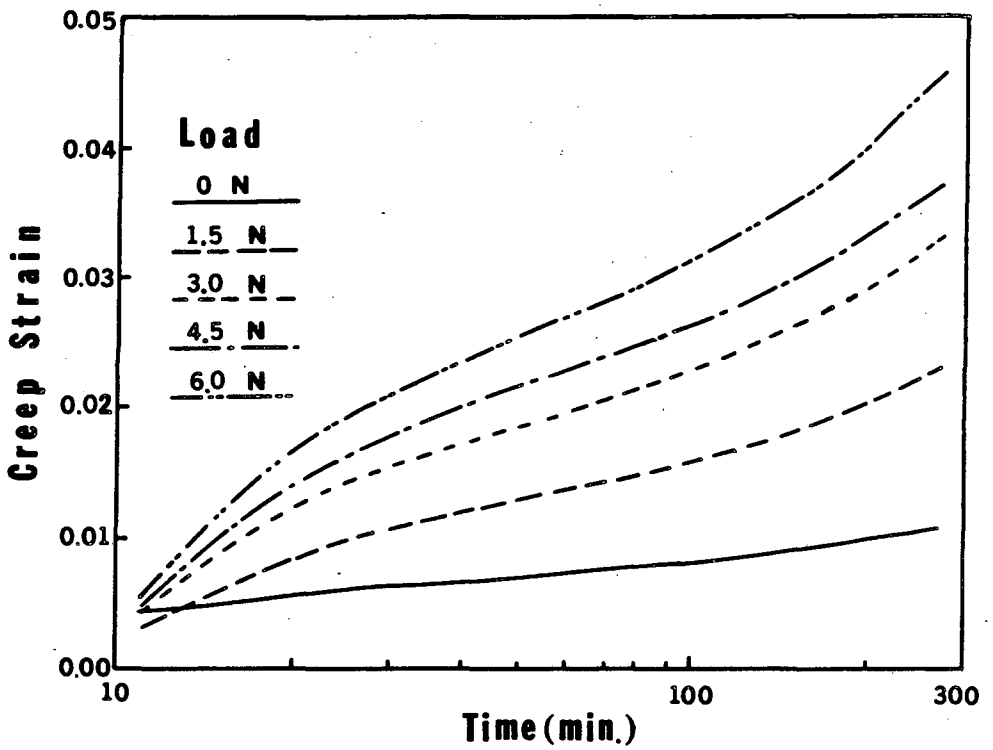

XBL 866-2191

Figure 4

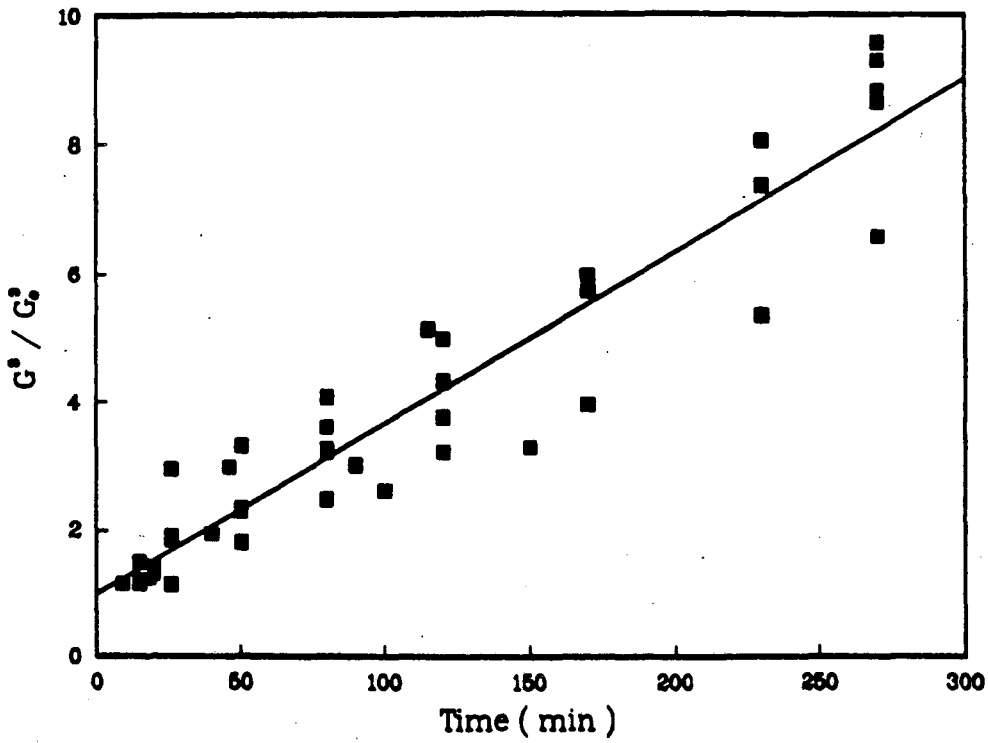

XBL 866-2192

Figure 5

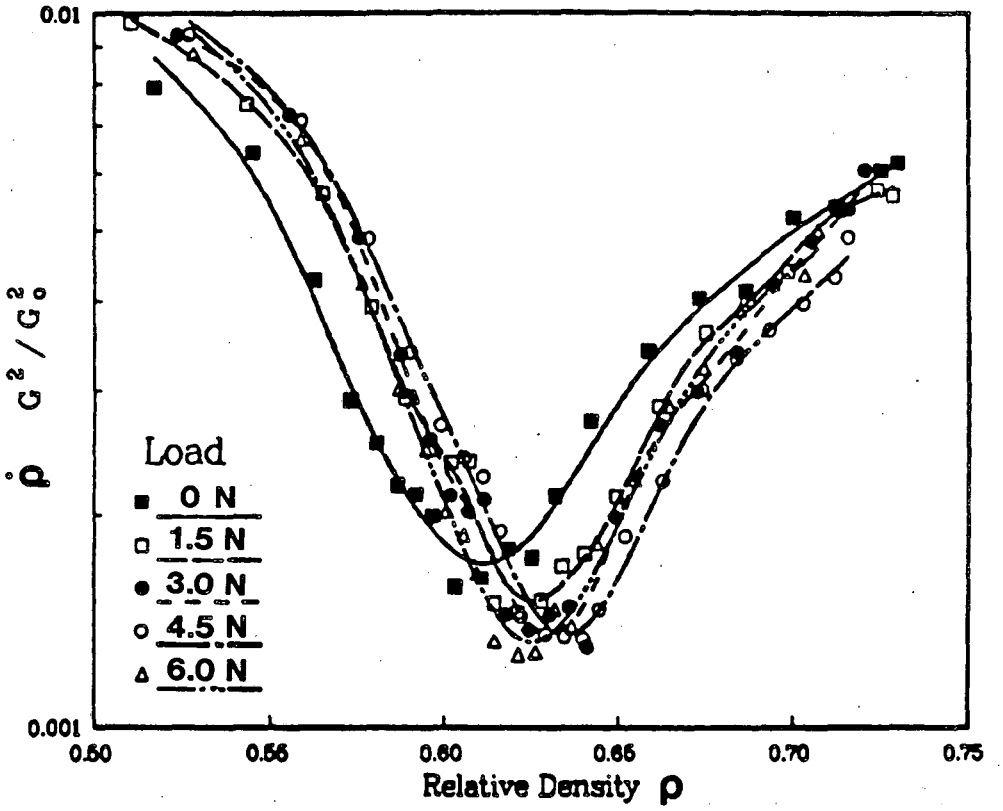

XBL 864-1649

Figure 6

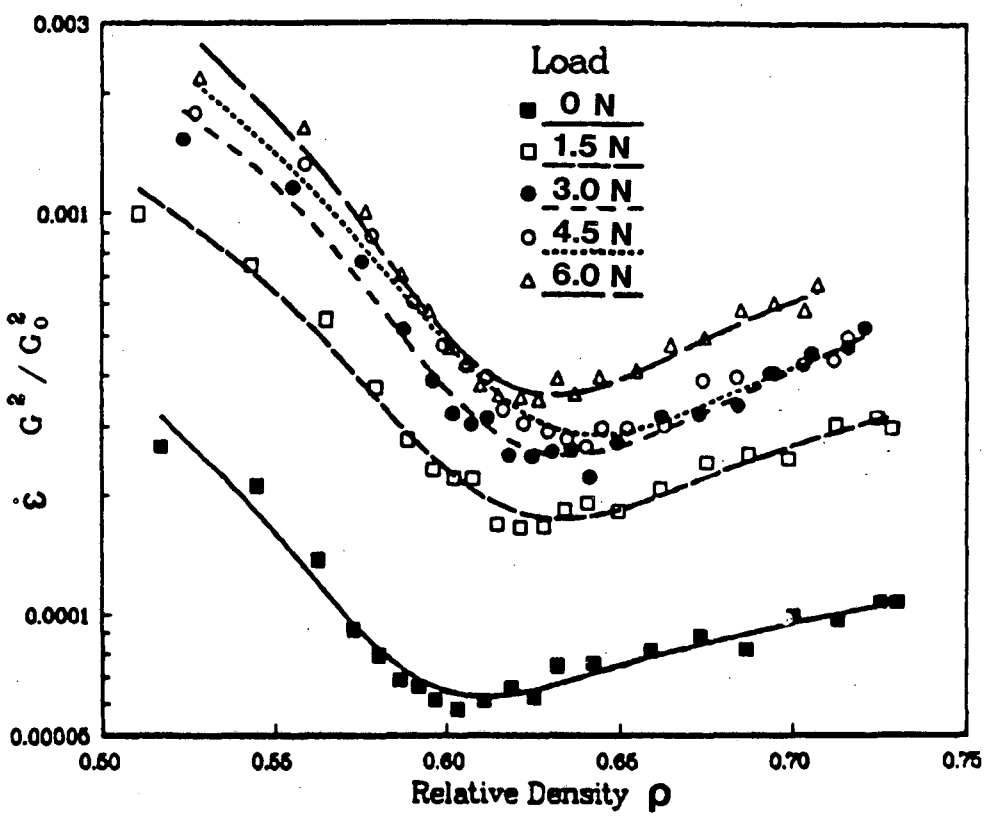

XBL 864-1651

Figure 7

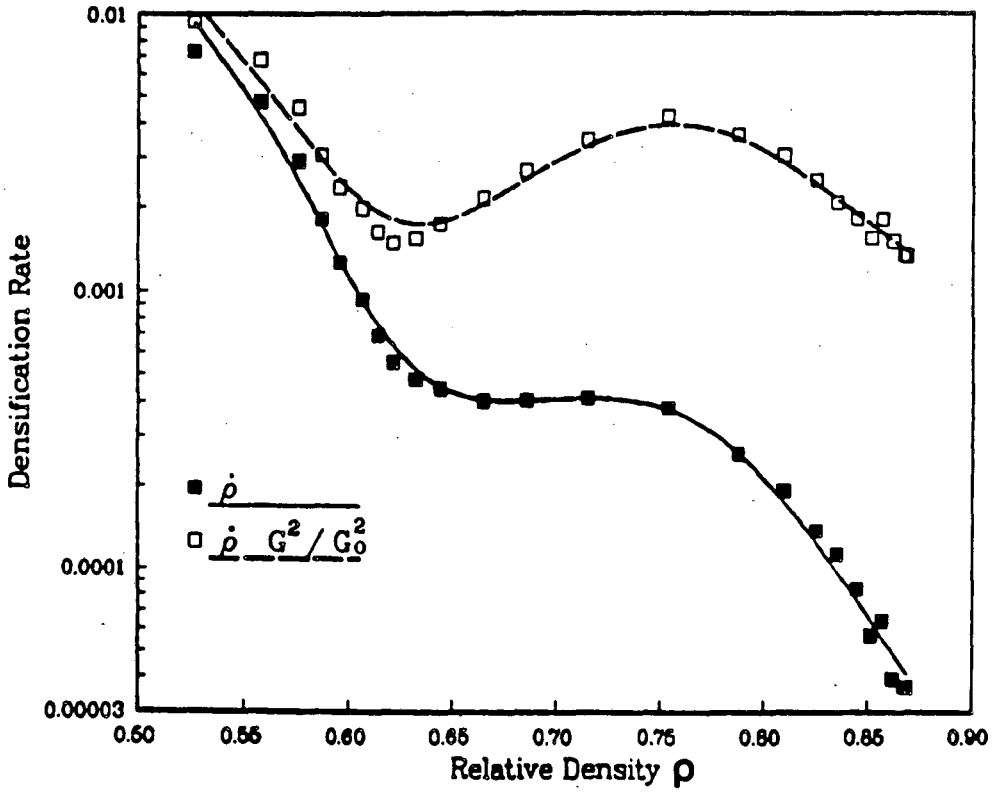

XBL 864-1650

Figure 8

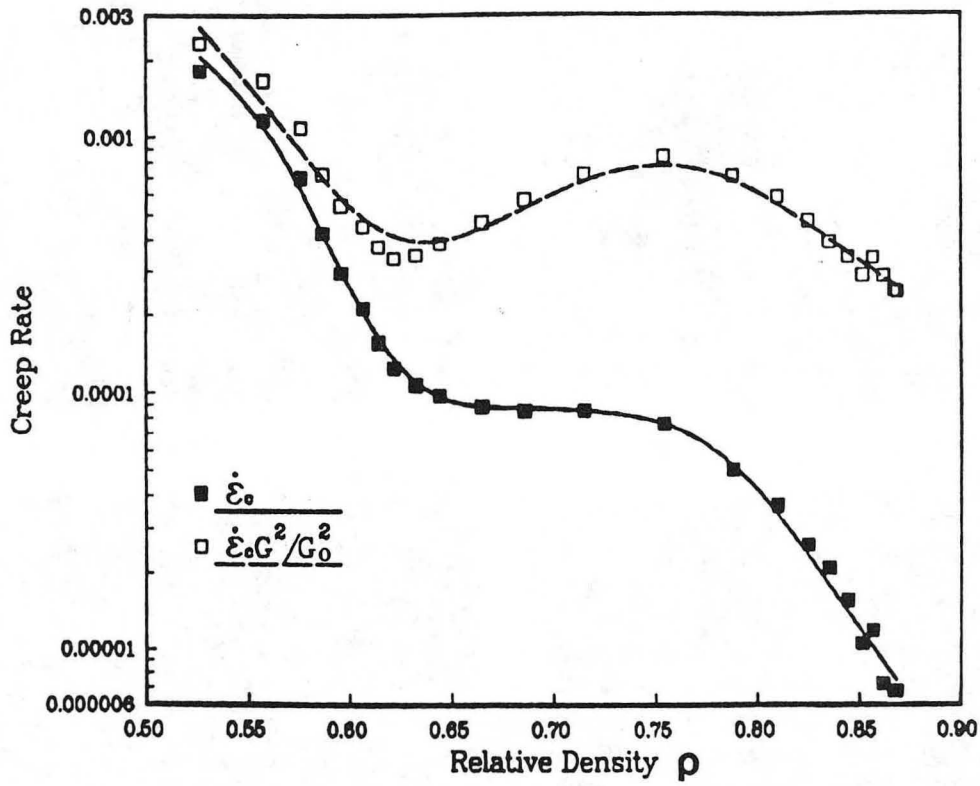

XBL 864-1652

Figure 9

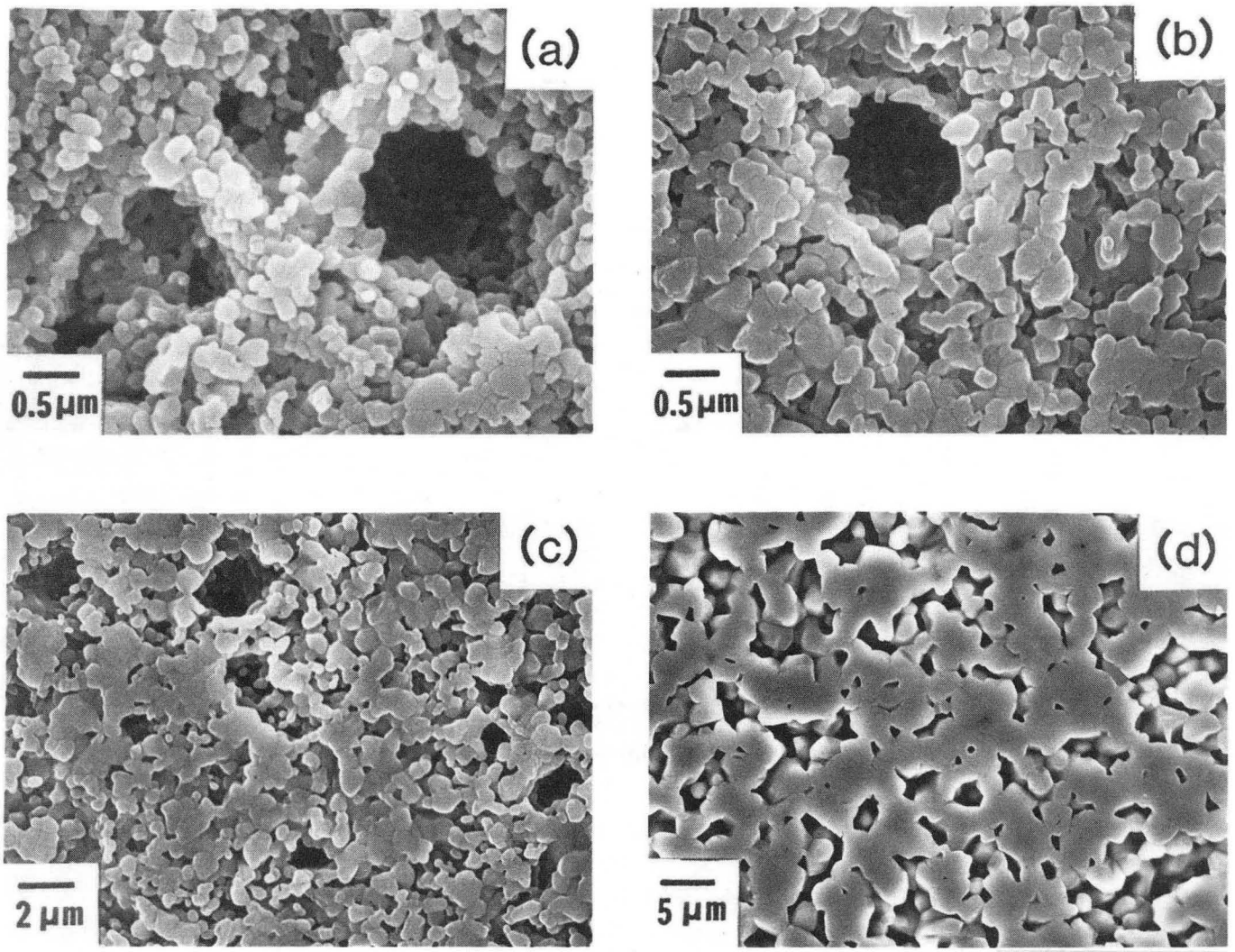

XBB 865-4299

Figure 10

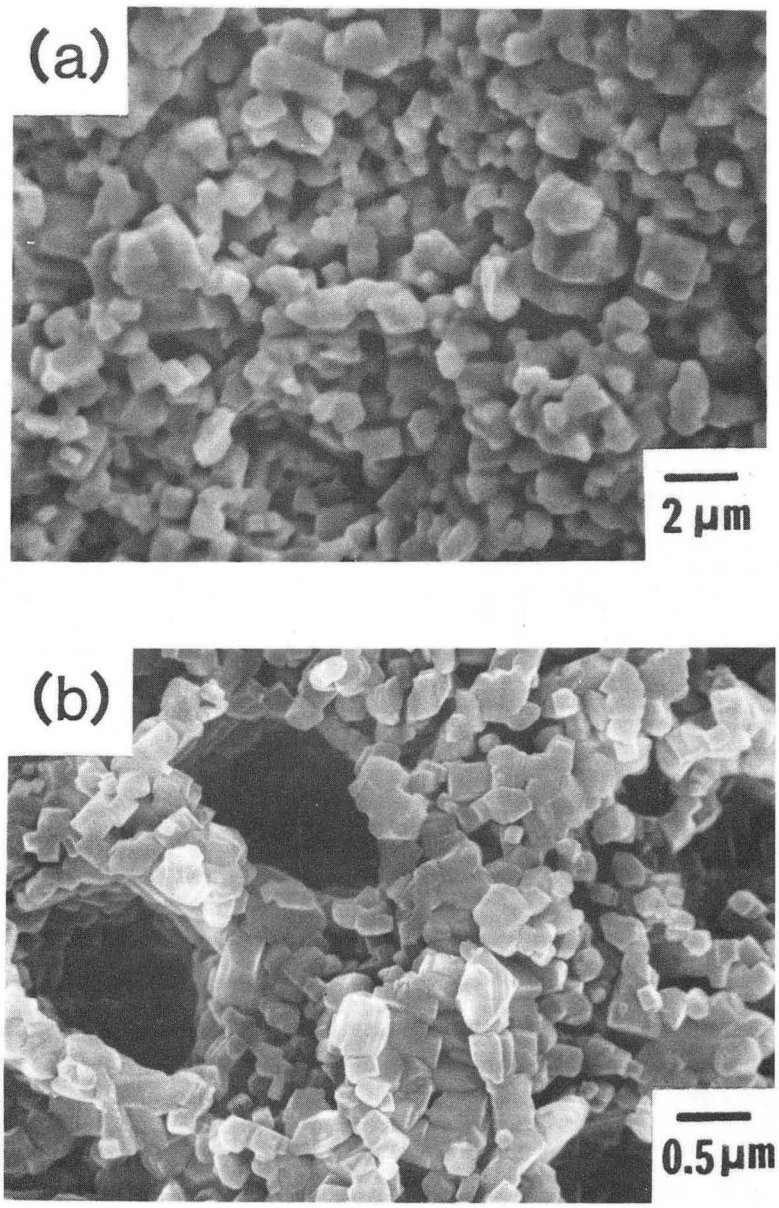

XBB 865-4300

Figure 11

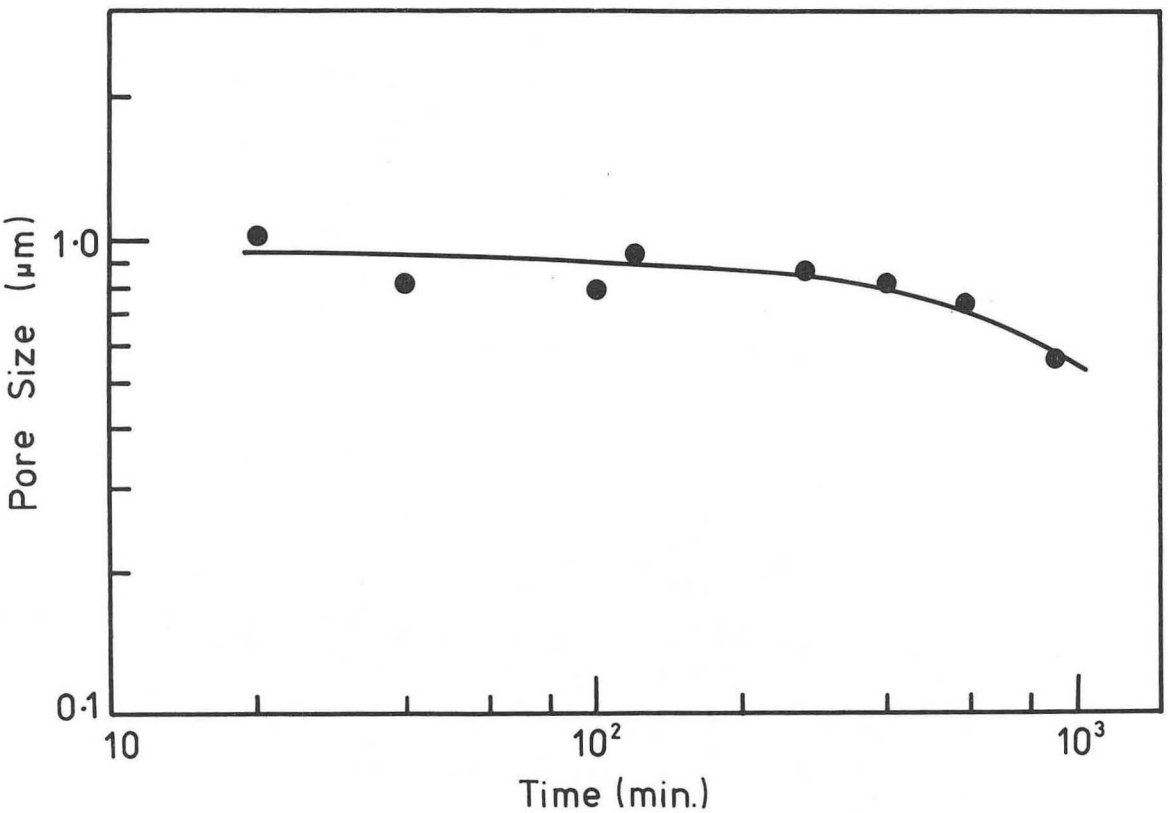

XBL 866-2517

Figure 12

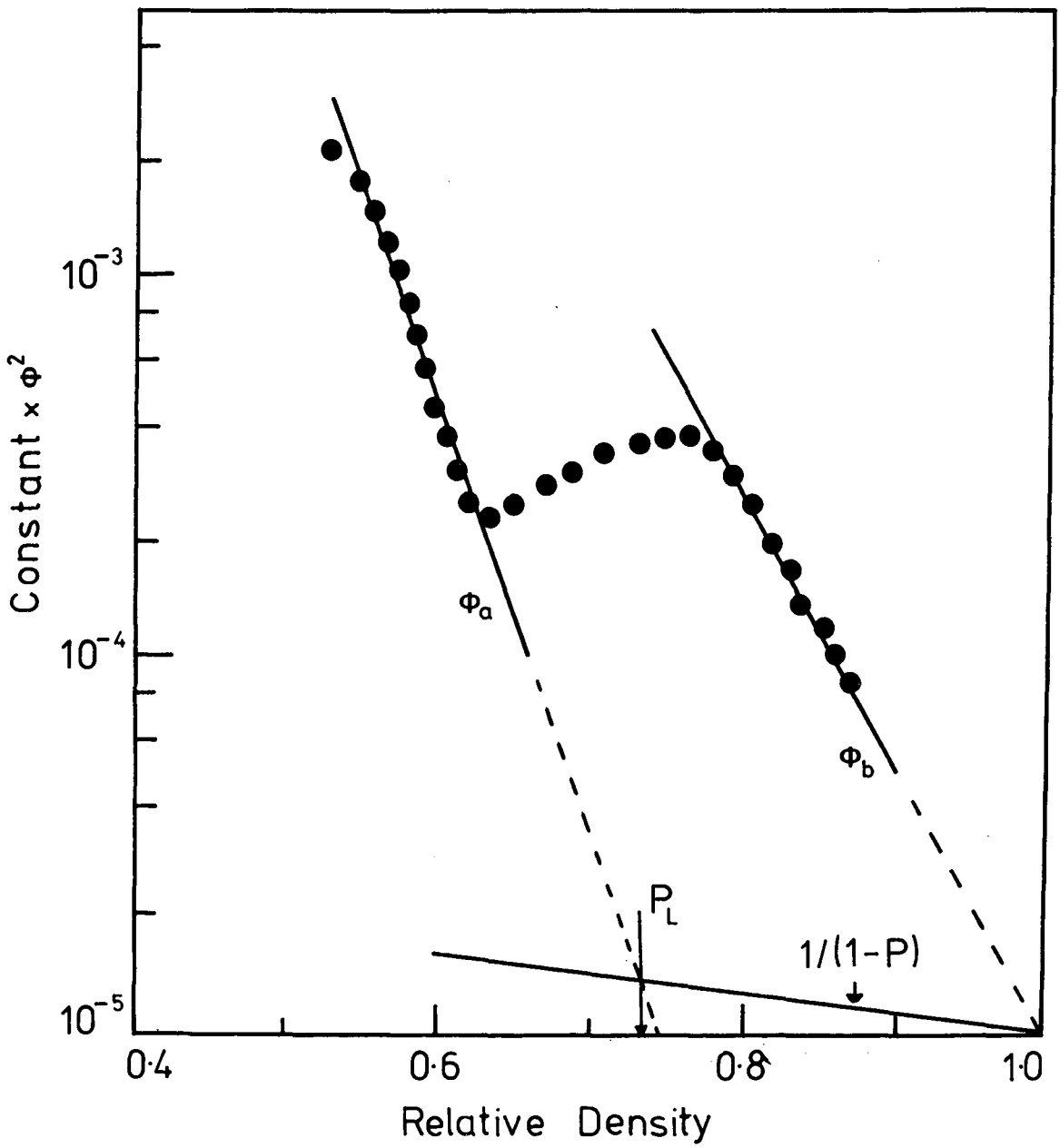

XBL 866-2516

Figure 13

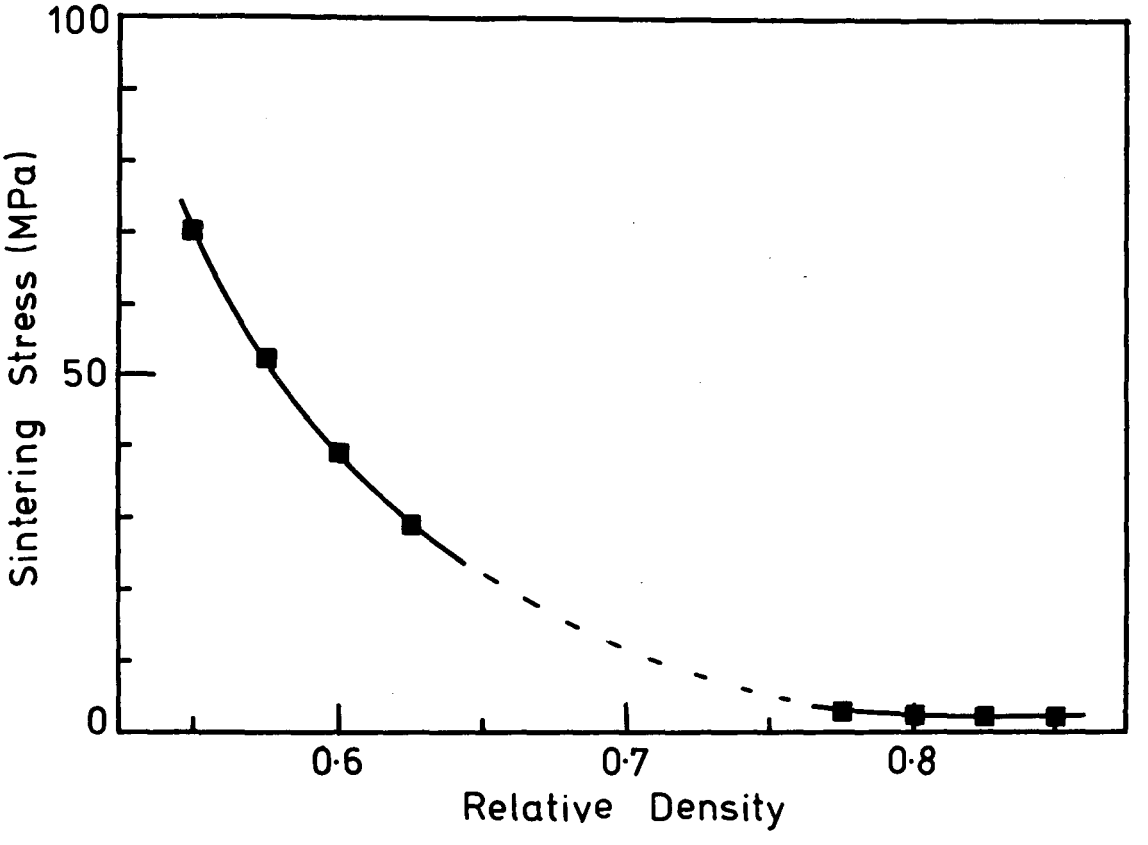

XBL 866-2518

Figure 14

This report was done with support from the Department of Energy. Any conclusions or opinions expressed in this report represent solely those of the author(s) and not necessarily those of The Regents of the University of California, the Lawrence Berkeley Laboratory or the Department of Energy.

Reference to a company or product name does not imply approval or recommendation of the product by the University of California or the U.S. Department of Energy to the exclusion of others that may be suitable.

LAWRENCE BERKELEY LABORATORY
TECHNICAL INFORMATION DEPARTMENT
UNIVERSITY OF CALIFORNIA
BERKELEY, CALIFORNIA 94720